Research Paper

Journal of Chemical Research

Journal of Chemical Research
1–11

DOI: 10.1177/1747519820907563
journals.sagepub.com/home/chl
SAGE

Synthesis, characterization, and biological properties of oxidovanadium(IV) complexes of acetylsalicylhydroxamic acid (*N*-acetyloxy-2-hydroxybenzamide) as potential antimicrobials

Bhanu Priya, Abhishek Kumar and Neeraj Sharma

Abstract

New oxidovanadium(IV) complexes of composition $[VO(AcSHA)_2]$ **1** and $[VO(acac)(AcSHA)]$ **2** are synthesized by reactions of $VOSO_4.5H_2O$ and $[VO(acac)_2]$ with acetylsalicylhydroxamic acid $AcSH_2A$ ($C_6H_4(OH)(CONHOCOCH_3)$) in a 1:2 molar ratio in absolute ethanol. The compounds are characterized by the Fourier-transform infrared spectroscopy, ultraviolet–visible spectroscopy, electron spin resonance, and mass spectrometry along with elemental analyses, molar conductivity, and magnetic moment measurements. The infrared spectra of the complexes suggest bonding through carbonyl and phenolic oxygen atoms (O,O coordination). The magnetic moment, electron spin resonance, and mass spectra of the complexes indicate that both exist as monomers, and a distorted square pyramidal geometry around vanadium is proposed. The thermal behavior of the complexes is studied by thermogravimetry and differential thermal analysis techniques under an N_2 atmosphere, yielding VO_2 as the decomposition product. The in vitro antimicrobial assays against pathogenic Gram-positive bacteria, Gram-negative bacteria, and fungi (minimum inhibitory concentration method) show the appreciable antimicrobial potential relative to the respective standard drugs, tetracycline hydrochloride, and fluconazole.

Keywords

acetylsalicylhydroxamic acid, biological properties, oxidovanadium(IV) complexes, spectral studies

Date received: 15 September 2019; accepted: 28 January 2020

Graphical abstract showing structure and antimicrobial activity of complex 1 and 2.

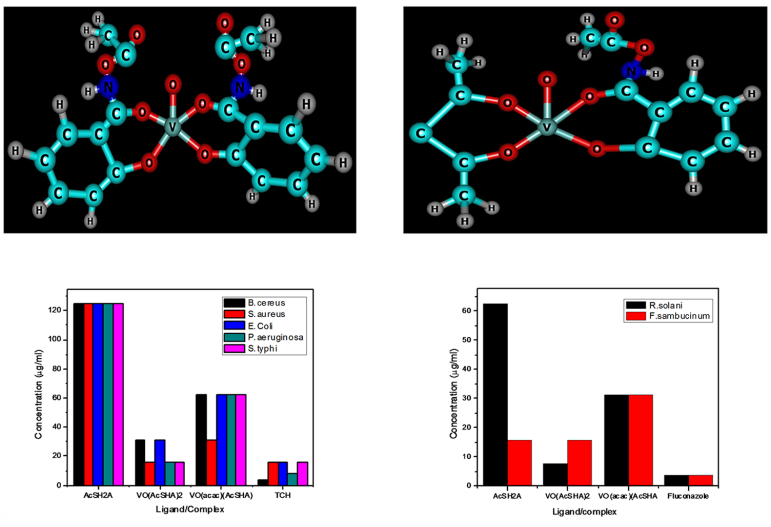

Department of Chemistry, Himachal Pradesh University, Shimla, India

Corresponding author:
Neeraj Sharma, Department of Chemistry, Himachal Pradesh University, Summer Hill, Shimla 171005, India.
Email: neerajsharma_univ@yahoo.co.in

Introduction

The ever-increasing research interest in oxidovanadium(IV) complexes is due to their prodigious biological and medicinal properties,[1–4] such as insulin-mimetic,[5–8] DNA binding and cleavage activity,[9–11] anticancer,[12] antioxidant,[13–15] antitrypanosomiasis,[16,17] antileishmaniasis,[18] antiamebiasis,[19] antituberculosis,[20] and anti-HIV[21] activity inducing apoptosis, inhibiting cell proliferation and preventing the metastasis of cancer against various cell lines.[22–24] The model studies related to vanadium biochemistry providing information on vanadium metabolism, toxicity, detoxification, and catalytic activity have been reported.[25] The bis(maltolato) (BMOV), bis(ethylmaltolato) (BEOV), and bis(allixinato)oxidovanadium(IV) are some of the most studied insulin-enhancing oxidovanadium(IV) complexes.[26–28] A drug containing vitamin A and vanadium(IV) salt having insulin-mimetic antidiabetic properties has been reported.[8] Oxidovanadium(IV) complexes as YopH tyrosine phosphatase inhibitors, a virulence factor produced by pathogenic species of *Yersinia*, have also been described.[29] The exponential progress in the medicinal chemistry of biologically relevant vanadium complexes for therapeutic applications is evident from numerous reports.[30–33]

On the contrary, hydroxamic acids with the functionality $R_CC(O)N(R_N)OH$ (R_C = alkyl/aryl; R_N = H or alkyl/aryl) are an important and key class of weak organic acids that have been well studied as bioligands. The distinctive chelating ability[34,35]—due to keto–enol tautomerism exhibited by the hydroxamic and hydroximic forms[36]—and the vast spectrum of pharmacological, toxicological, and pathological properties of hydroxamic acids have fascinated researchers in the design of new complexes of biological relevance.[37–39]

Biologically significant acetylated hydroxamic acids synthesized from salicylhydroxamic acid using various acetylating agents and different methodologies have been reported.[40,41] The reaction of salicylhydroxamic acid with acetyl chloride in the presence of pyridine and ethyl acetate forms acetylsalicylhydroxamic acid ($AcSH_2A$) where $AcSH_2A = C_6H_4(OH)(CONHOCOCH_3)$, and the acetyl group is located on the hydroxamic acid group. The vanadium hydroxamate complexes derived from acetohydroxamic acid (aceto-HAha), benzohydroxamic acid (HBha), *N*-phenylbenzohydroxamic acid, 2-hydroxypyridine *N*-oxide,[42] nicotinohydroxamato, 4-nitrobenzohydroxamate, and 2-chloro-4-nitrobenzohydroxamate ligands are also well-documented.[43,44]

As a part of our continuing work on vanadium hydroxamates,[45–47] we herein report the synthesis of new bis(acetylsalicylhydroxamato) and the mixed-ligand (acetylacetonato)(acetylsalicylhydroxamato)oxidovanadium(IV) complexes using two different vanadium precursors along with their characterization by the Fourier-transform infrared spectroscopy (FTIR), ultraviolet–visible spectroscopy (UV-Vis), electron spin resonance (ESR), and mass spectral techniques. The electrochemical and thermal behavior of the complexes has also been studied. The antimicrobial and antioxidant potential of the complexes has been assayed against some pathogenic bacteria and fungi by minimum inhibitory concentration (MIC) method and DPPH (1,1-diphenyl-2-picrylhydrazyl) free radical scavenging method, respectively.

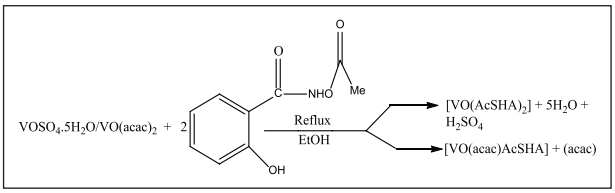

Scheme 1. Synthesis of oxidovanadium(IV) complexes.

Results and discussion

The reactions of $VOSO_4.5H_2O$ and $VO(acac)_2$ with 2 equiv. of $AcSH_2A$ in absolute ethanol in separate experiments gave dark blue complexes of composition $[VO(AcSHA)_2]$ **1** and [VO(acac)(AcSHA)] **2**, respectively, in quantitative yields and are consistent with their elemental analysis (Scheme 1).

The molar conductance values of the complexes measured in methanol were 3.92 and 3.90 $Scm^2\,mol^{-1}$, respectively, suggesting their non-electrolytic nature.[48] At the room temperature, magnetic moment of 1.70 and 1.72 BM (Bohr magneton) for complexes **1** and **2** is well within the range reported for monomeric oxidovanadium(IV) complexes.[49]

Infrared spectra

A comparison of the infrared (IR) spectra of the complexes with that of the ligand supports their formation. Free $AcSH_2A$ exhibited bands due to $\nu(OH)_{phenolic}$, ν(N–H), $\nu(C{=}O)_{acetyl}$, $\nu(C{=}O)_{hydroxamic}$, ν(C–N), and ν(N–O) modes at 3423, 3345, 1773, 1645, 1348, and 954 cm^{-1}, respectively, whereas the complexes $[VO(AcSHA)_2]$ and [VO(acac)(AcSHA)] displayed the respective bands at 3274, 1770, 1603, 1371, and 907 cm^{-1} and 3392, 1770, 1660–1626, 1348–1342, and 917 cm^{-1}, as presented in Tables 1 and 2, respectively.

The nonobservance of the band due to the ν(OH) mode in complexes **1** and **2** is indicative of deprotonation of the phenolic hydrogen, involving bonding through the phenolic oxygen. The $\nu(C{=}O)_{hydroxamic}$ mode in complex **1** shifted to a lower wavenumber by 42 cm^{-1} and the ν(C–N) mode shifted to a higher wavenumber by 23 cm^{-1} as compared to the ligand. The absorption band due to $\nu(C{=}O)_{acetyl}$ occurred at 1770 cm^{-1}, showing an insignificant shift from the ligand and suggesting the nonparticipation of the acetyl group in bonding (see Figure S1(a)–(c) in the supporting information). The shift in the ν(N–O) mode to a lower wavenumber by 47 cm^{-1} is contrary to earlier reports wherein the ν(N–O) mode shifts to a higher wavenumber upon complexation. The occurrence of the ν(N–H) mode is suggestive of its retention upon complexation. The absorption bands due to the ν(V=O) mode occurred at 970 and 957 cm^{-1}, respectively. However, this observation is in contrast to those for Co(II), Ni(II), Cu(II), and Zn(II) complexes of $AcSH_2A$ wherein tridentate bonding behavior of ligand has been reported.[40]

Table 1. IR spectral data of the ligand ($AcSH_2A$) and the complexes **1** and **2**.

Ligand/complex	Bands (cm^{-1})
($AcSH_2A$)	3423, 3345, 3189, 3071, 1773, 1645, 1625, 1596, 1537, 1486, 1348, 1307, 1244, 1141, 1123, 1030, 954, 864, 748, 675, 637, 578, 502, 445, 419
[$VO(AcSHA)_2$]	3274, 3050, 2941, 2866, 2729, 2583, 1770, 1603, 1463, 1371, 1308, 1231, 1185, 1156, 1097, 1051, 1031, 970, 907, 857, 782, 744, 688, 596, 546, 461, 422
[VO(acac)(AcSHA)]	3392, 3182, 3071, 2793, 2464, 1770, 1660, 1626, 1596, 1490, 1348, 1342, 1213, 1154, 1119, 1032, 1012, 957, 917, 867, 748, 676, 578, 504, 444

Table 2. Important IR frequencies (cm^{-1}) of the ligand ($AcSH_2A$) and the complexes **1** and **2**.

Ligand/complex	$\nu(OH)_{hydroxamic}$	ν(N–H)	$\nu(C=O)_{acetyl}$	$\nu(C=O)_{hydroxamic}$	ν(C–N)	ν(N–O)
(AcSHA)	3423	3345	1773	1645	1348	954
[$VO(AcSHA)_2$]	–	3274	1770	1603	1371	907
[VO(acac)(AcSHA)]	–	3392	1770	1660–1626	1348–1342	917

Table 3. UV-Vis spectral data of the ligand ($AcSH_2A$) and the complexes **1** and **2.**

Ligand/complex	Λ (nm)
($AcSH_2A$)	319
[$VO(AcSHA)_2$]	270, 308, 478, 735
[VO(acac)(AcSHA)]	305, 316, 425, 720

Table 4. Mass spectral data of the complex [$VO(AcSHA)_2$] **1**.

Complex	m/z	Intensity (%)
$[VO(AcSHA)_2 + Na]^+$	479	4.3
$[VO(AcSHA)_2 - 6H]^+$	451	21.7
[2AcSHA]	390	8.6
$[2(AcSHA) - 2CH_3 - 4H]^+$	354	60.8
$[VO(AcSHA)]^+$	262	34.7
$[AcSHA + K]^+$	234	20
$[AcSHA + Na]^+$	218	100

Electronic spectra

The UV-Vis spectra of the ligand ($AcSH_2A$) recorded in absolute ethanol displayed an absorption band at 319 nm attributed to an intra-ligand $\pi \rightarrow \pi^*$ transition. Complexes **1** and **2** exhibited bands at 270, 308, 478, and 735 nm and 305, 316, 425, and 720 nm in the UV-Vis region, respectively (Table 3). The high-energy intra-ligand bands at 270 and 308 nm and 305 and 316 nm occurred in complexes **1** and **2**, respectively, are contrary to previous reports.[49,50] The bands appeared in the visible region may be assigned to $^2B_2 \rightarrow {}^2A_1$ ($3dxy \rightarrow 3dz^2$) and $^2B_2 \rightarrow {}^2E$ ($3dxy \rightarrow 3dxz$, $3dyz$) d–d transitions, respectively, and a plausible square pyramidal geometry around vanadium is proposed.[51,52]

Mass spectra

The electrospray ionization (ESI) mass spectrum of complex **1** exhibited a molecular ion peak at m/z (%), that is, 479 (4.3), corresponding to $[VO(AcSHA)_2 + Na]^+$. The most abundant peak at 218 (100) corresponded to $[AcSHA + Na]^+$, which is presented in Table 4.

The other structurally important fragment ions at m/z (%) 451 (21.7), 390 (8.6), 354 (60.8), 262 (34.7), and 234 (20) corresponded to $[VO(AcSHA)_2 - 6H]^+$, [2AcSHA], $[2AcSHA - 2CH_3 - 4H]^+$, $[VO(AcSHA)]^+$, and $[AcSHA + K]^+$, respectively, as clearly shown in Scheme 2 (see Figure S2 in the supporting information).

The mass spectrum of complex **2** displayed the molecular ion and the base peak at m/z (%) 360 (18) and 302 (100) corresponding to [VO(acac)(AcSHA)] and [VO(acac)(AcSHA)$-OCOCH_3-H]^+$, respectively (Table 5).

The other fragment ions at m/z (%) 230 (25.4) and 202 (21.8) corresponded to $[AcSHA + K^+ - 4H]^+$ and $[VO(acac) + K^+ - 3H]^+$, respectively (Scheme 3) (see Figure S3 in the supporting information).

ESR spectra

At the room temperature, X-band ESR spectra of complexes **1** and **2** displayed the well-resolved typical eight lines due to the interaction of an unpaired electron of the vanadium(IV) center with its own nucleus, that is, I = 7/2 indicative of the mononuclear oxidovanadium(IV). The nuclear magnetic quantum numbers analogous to these lines are −7/2, −5/2, −3/2, −1/2, +1/2, +3/2, +5/2, and +7/2 from low to high field. The complex **1** showed $\mathbf{g}\| = 1.94$ and $\mathbf{A}\|$ ($\times 10^{-4}\,cm^{-1}$) = 163 and $\mathbf{g}^{\perp} = 1.98$ and $\mathbf{A}^{\perp}$ ($\times 10^{-4}\,cm^{-1}$) = 65. The complex **2** exhibited $\mathbf{g}\| = 1.96$ and $\mathbf{A}\| = 161$ and $\mathbf{g}^{\perp} = 1.98$ and $\mathbf{A}^{\perp} = 67$. The g_{iso} values calculated from the spectra for complexes **1** and **2** of same magnitude 1.96 are close to the spin-only value (free electron value of 2.0023; Table 6).

The observed order $\mathbf{A}\| > \mathbf{A}^{\perp}$ and $\mathbf{g}^{\perp} > \mathbf{g}\|$ suggests that the unpaired electron lies in the d_{xy} orbital corresponding to the square pyramidal geometry around vanadium in complexes **1** and **2** in agreement with the reports on oxidovanadium(IV) chelates.[53,54]

Cyclic voltammetry

The free ligand ($AcSH_2A$) displayed one reductive wave and one oxidative wave at −0.61 and −0.51 V, respectively. The complex **1** exhibited two reduction waves at −0.48 and

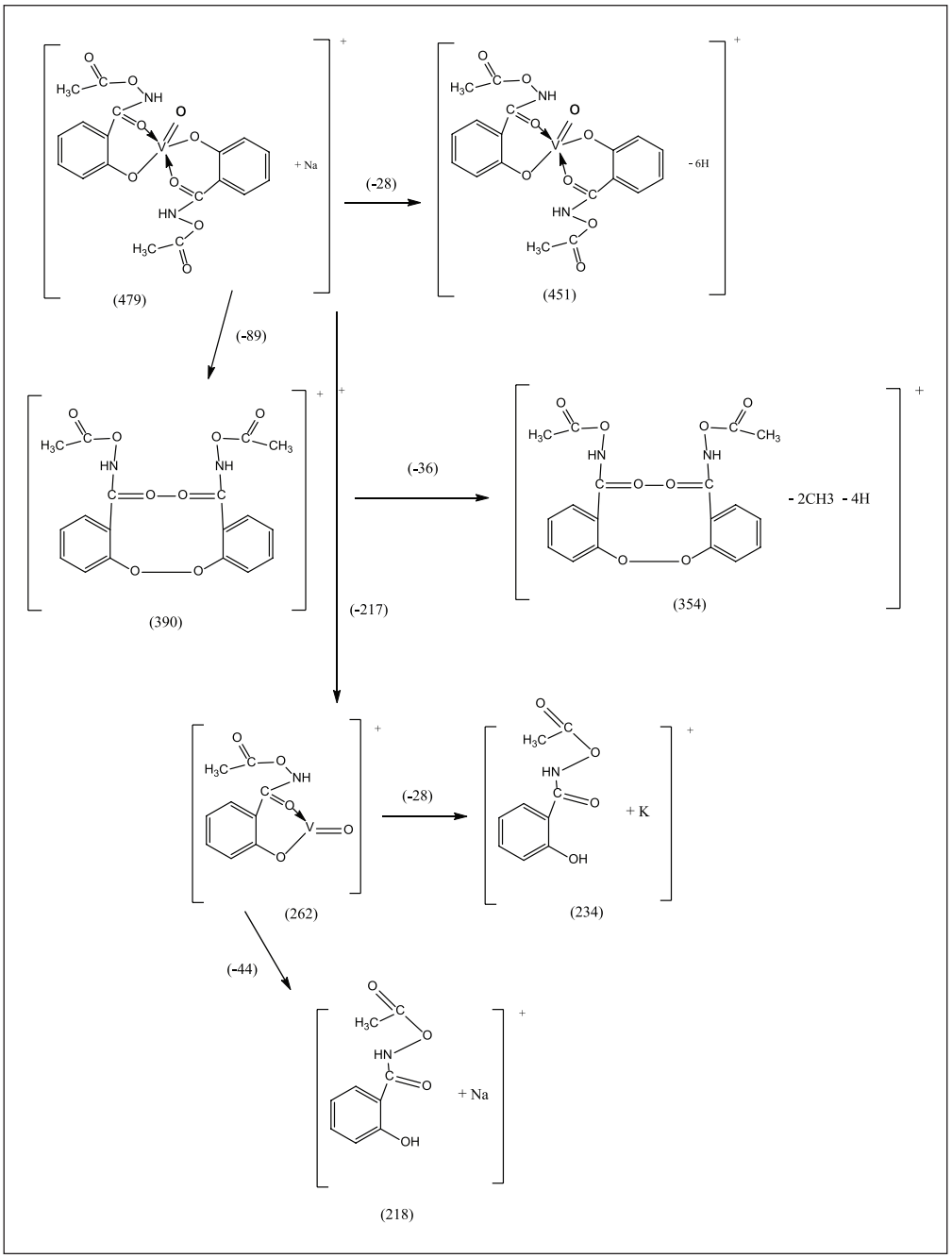

Scheme 2. Mass spectral fragmentation pattern of complex **1.**

Table 5. Mass spectral data of complex [VO(acac)(AcSHA)] **2**.

Complex	m/z	Intensity (%)
[VO(acac)(AcSHA)]	360	18
$[VO(acac)(AcSHA) - OCOCH_3 - H]^+$	302	100
$[AcSHA + K^+ - 4H]^+$	230	25.4
$[VO(acac) + K^+ - 3H]^+$	202	21.8

+0.69 V and one oxidation wave at −0.551 V. The complex [VO(acac)(AcSHA)] **2** exhibited reductive and oxidative waves at +0.62 and −0.26 V, respectively (Table 7 and Figures 1–3).

The peak-to-peak separation value ($\Delta E_p = 79$ mV) is indicative of a single-step pseudo-reversible one-electron transfer process and also adjudged from the peak current ratio I_{pa}/I_{pc}. The electrode process can be represented as

$$\left[VO^{IV}L\right] \rightarrow \left[VO^{V}L\right]$$

The $E_{1/2}$ value of 519 mV may be assigned to metal-centered oxidation of V^{IV} to V^{V} lying within the range reported for related complexes.[55] Based upon physicochemical and various spectral techniques, a distorted square pyramidal geometry in both the mononuclear complexes has been proposed around the vanadium (Figures 4 and 5).

Thermogravimetric studies

The complexes **1** and **2** have shown the thermal stability up to 60°C and 85°C, respectively, after which these

complexes went decomposition in two steps. The mass loss of 45% in the first step in complex **1** in the temperature range of 60°C–427°C analogous to the dissociation of one acetylsalicylhydroxamate ligand yielding [VO(AcSHA)] as the likely unstable intermediate. The mass loss of 36.9% in the second step, between 427°C and 646°C, accounted for the decomposition of another $AcSH_2A$ ligand to yield VO_2 as the final residue. The formation of VO_2 as thermolyzed product of vanadium(IV) hydroxamate complexes has been authenticated by recording the IR spectra of the residue. The sharp absorption bands appeared at ~992 cm^{-1} due to ν(V=O) mode and the other bands appeared at 675, 658, 620, 520, and 322 cm^{-1} are in line with earlier reports on the IR spectra of VO_2.[56] The thermal decomposition pattern of complex **1** is presented in Scheme 4.

A broad exothermic peak at 556.0°C in differential thermal analysis (DTA) curve corroborated thermal decomposition in thermogravimetry. The mass loss of 57.73% in complex **2** in the first step in the temperature range of 85°C–400°C accounted for the removal of one acetylsalicylhydroxamate ligand yielding [VO(acac)] as the probable unstable intermediate. The mass loss of 27.57% in the second step, between 400°C and 617°C corresponded to the decomposition of the acetylacetonate ligand to yield VO_2 as the final residue. The thermal decomposition pattern of complex **2** is presented in Scheme 5.

The two-step decomposition in the thermogravimetric analysis (TGA) is accompanied by an exothermic inflection at 133°C and a broad peak at 577°C in the DTA curve (Table 8 and Figures 6 and 7).

Biological studies

Literature contains numerous reports on the transport of the pharmacologically active vanadium(IV) and (V) complexes as well as the role of the ligand in various redox and uptake processes, wherein the active species formed depend upon the thermodynamic stability of vanadium complexes and the potential of ligand to cross the cell membrane in bodily fluids at physiological pH.[57–69] The oxidovanadium(IV) hydroxamates[43,45–47,70,71] have drawn considerable attention owing to their interesting biological activity over the last few years. In pursuit of new vanadium-based antimicrobials, the antimicrobial activity of the complexes **1** and **2** has been assayed.

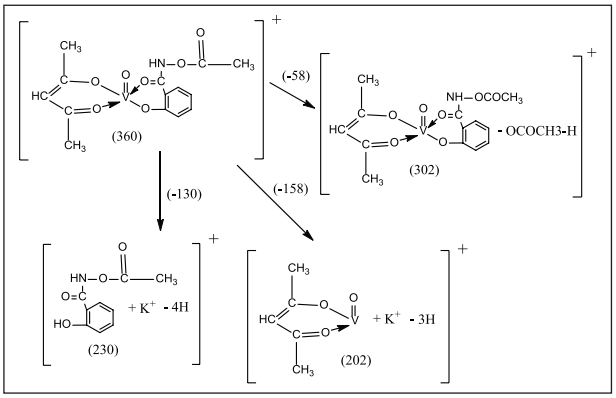

Scheme 3. Mass spectral fragmentation pattern of complex **2.**

Antibacterial activity. The uncoordinated ligand ($AcSH_2A$) showed inhibitory effects against the test bacteria at MIC 125 μg/mL. The complex **1** affected the growth inhibition of *Bacillus cereus* and *Escherichia coli* at MIC 31.25 μg/mL, while that of *Staphylococcus aureus, Pseudomonas aeruginosa*, and *Salmonella typhi* occurred at 15.63 μg/mL, which may be attributed to the difference in the diffusion of the complex through the cell wall of these bacteria. The complex **2** has been found to be quite effective against *E. coli* and *S. typhi* at MIC 31.25 μg/mL compared to *B. cereus, P. aeruginosa*, and *S. aureus* at 62.5 μg/mL. The reference drug tetracycline hydrochloride inhibited test bacteria at MIC 3.90–15.63 μg/mL (Table 9 and Figure 8).

The complex **1** is quite effective against all the test bacteria and highly effective against *B. cereus* better than the standard drug. The growth inhibition by complex **1** is prominent against *S. aureus* (Gram-positive) and *S. typhi* (Gram-negative) relative to the free ligand and the complex **2**. The enhanced inhibitory activity of the complexes can be ascribed to the reduction of the polarity in the metal ion and increased delocalization of π electrons over the whole chelate ring, thereby increasing the lipophilicity and allowing efficient diffusion of the complex into the bacterial cell wall.[72,73]

Antifungal activity. The antifungal activity of the free ligand and the complexes **1** and **2** has been studied against *Rhizoctonia solani* and *Fusarium sambucinum*. The ligand ($AcSH_2A$) inhibited these fungi with MIC values of 62.5 and 15.62 μg/mL, respectively. The complexes **1** and **2** have shown enhanced inhibitory effects against the test fungi at MIC values of 7.81, 15.62, and 31.25 μg/mL, respectively (Table 10 and Figure 9). The standard drug fluconazole inhibited these fungi at MIC 3.90 μg/mL.

Antioxidant activity. The antioxidant activity of the free ligand and the complexes **1** and **2** studied by the DPPH method showed a low scavenging potential (~4.9%–26.3%) for the ligand, which was significantly enhanced (~29.4%–45.3% and ~10.4%–43.28%) in complexes through the oxidation of $V(IV)O^{2+}$ to $V(V)O^{+}$. The

Table 6. ESR spectral data of oxidovanadium(IV) complexes **1** and **2.**

Complex	g‖	$g^{\perp}$	$\Delta g = g^{\perp} - g\|\|$	$g_{iso} = \frac{2g^{\perp} + g\|\|}{3}$	A‖ (×10^{-4} cm^{-1})	$A^{\perp}$ (×10^{-4} cm^{-1})
$[VO(AcSHA)_2]$	1.94	1.98	0.04	1.96	163	65
[VO(acac)(ACSHA)]	1.96	1.97	0.01	1.96	161	67

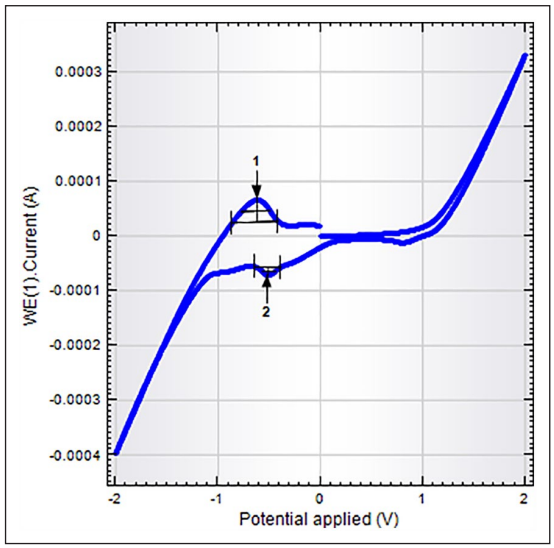

Figure 1. Cyclic voltammogram of the free ligand ($AcSH_2A$).

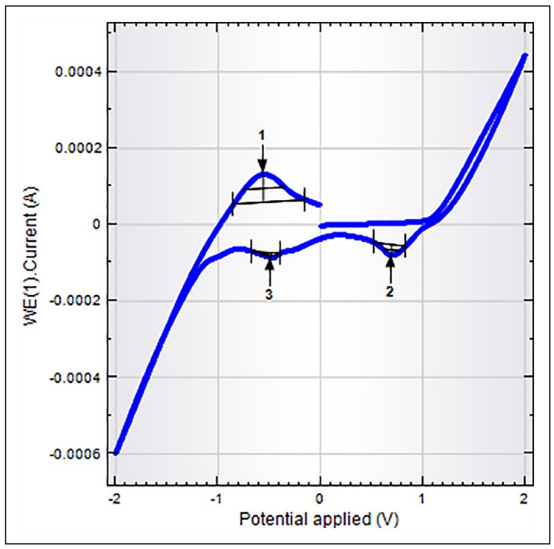

Figure 2. Cyclic voltammogram of the complex **1** $[VO(AcSHA)_2]$.

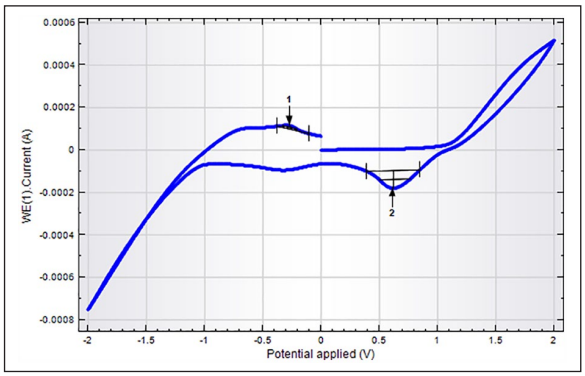

Figure 3. Cyclic voltammogram of the complex **2** [VO(acac)(ACSHA)].

complex **1** exhibited high activity compared to the free ligand and the complex **2** (Table 11).

This is in agreement with the fact that large conjugated systems upon chelation with metal ions promote the

Table 7. Cyclic voltammetric data of ligand ($AcSH_2A$) and oxidovanadium(IV) complexes **1** and **2.**

Ligand/complex	E_{pa} (V)	E_{pc} (V)	ΔE (V)	I_{pa} (A)	I_{pc} (A)	I_{pa}/I_{pc}
($AcSH_2A$)	−0.51	+0.61	1.110	0.85	3.83	0.22
$[VO(AcSHA)_2]$	−0.551	+0.690	−1.250	1.25	4.01	0.31
[VO(acac)(AcSHA)]	−0.260	+0.62	−0.880	3.30	5.09	0.65

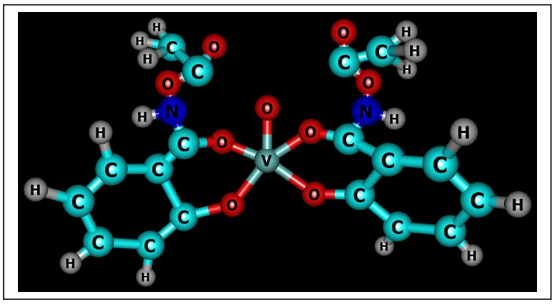

Figure 4. Chemcraft structure of the complex **1** $[VO(AcSHA)_2]$.

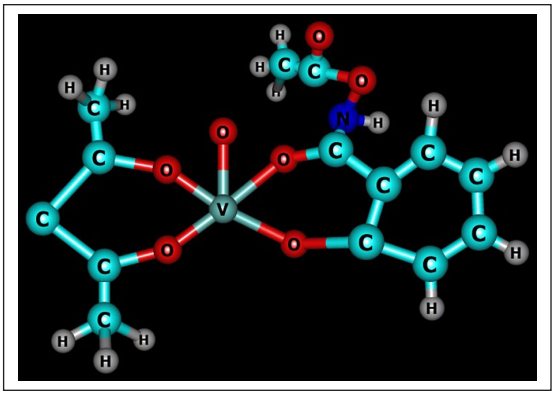

Figure 5. Chemcraft structure of the complex **2** [VO(acac)(ACSHA)].

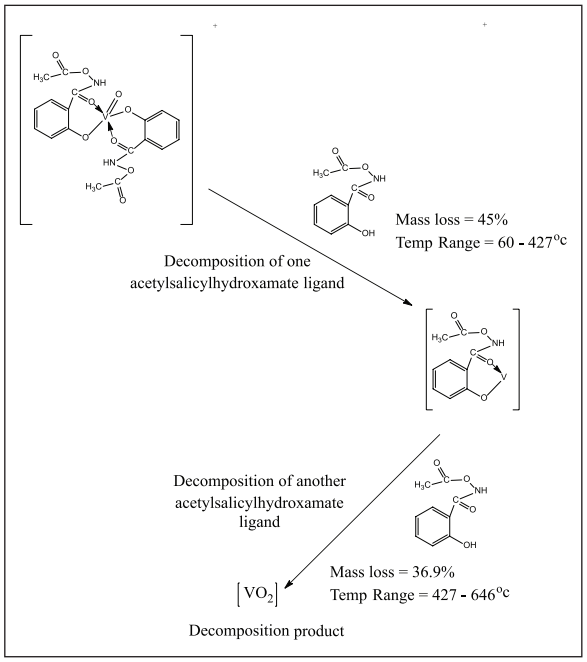

Scheme 4. Thermal decomposition pattern of complex **1.**

trapping of free radicals, which results in discoloration from the purple DPPH radical solution to a yellow solution showing scavenging of DPPH radicals by hydrogen donation.

Conclusion

The oxidovanadium(IV) complexes of composition $[VO(AcSHA)_2]$ and [VO(acac)(AcSHA)] derived from acetylsalicylhydroxamic acid $[C_6H_4(OH)CONHOCOCH_3]$ have been synthesized and thoroughly characterized by various physicochemical and spectroscopic techniques (FTIR, UV-Vis, ESR) and mass spectrometry. IR data showed the disappearance of the $\nu(OH)_{phenolic}$, lowering of the $\nu(C{=}O)_{hydroxamic}$, and a shift of the ν(N–O) and ν(C–N) modes to a higher frequency, without any significant change in $\nu(C{=}O)_{acetyl}$. This indicates that the acetylsalicylhydroxamic acid acts as a bidentate chelating ligand involving bonding through carbonyl and phenolic oxygen atoms (O,O). From spectral studies, a distorted square pyramidal geometry may tentatively be proposed around vanadium. The complexes are electrochemically active and exhibit single-step pseudo-reversible one-electron transfer processes. The thermal behavior of complexes **1** and **2** studied by the thermogravimetric technique and showed a two-step decomposition to yield VO_2 as the residue. The in vitro antibacterial assay of the free ligand and the complexes **1** and **2** has shown that the growth inhibition by complex **1** is prominent against *S. aureus* (Gram-positive) and *S. typhi* (Gram-negative) relative to the free ligand and the complex **2**. The in vitro antifungal activity of the ligand and complexes evaluated against *R. solani* and *F. sambucinum* showed that the complex **1** exhibits good inhibitory effects against both the fungi in contrast to complex **2**. The results reveal these new complexes as promising antimicrobial agents to be explored further for medicinal applications. It has been further elucidated that the complex **1** exhibited high antioxidant activity compared to the free ligand and the complex **2**.

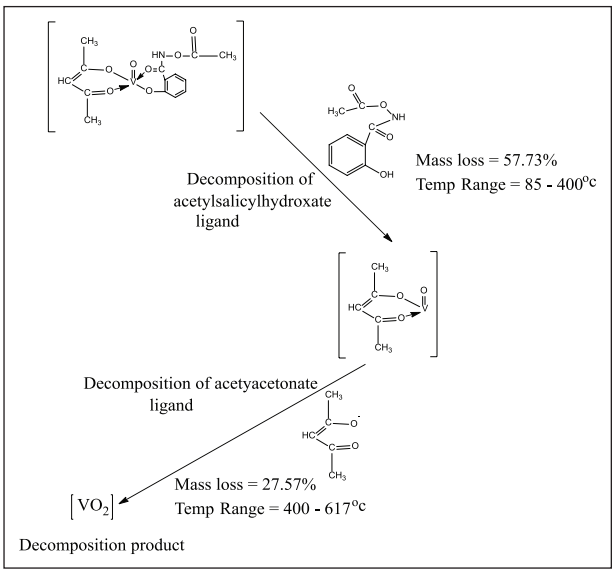

Scheme 5. Thermal decomposition pattern of complex **2.**

Experimental details

Materials and methods

All chemicals of reagent grade were used. Vanadyl sulfate ($VOSO_4.5H_2O$; Merck) was used as procured. $[VO(acac)_2]$ and acetylsalicylhydroxamic acid $[C_6H_4(OH)CONHOCOCH_3]$ were synthesized by reported methods,[74,75] and characterized by microanalyses and IR spectroscopy. The vanadium content in the complexes was

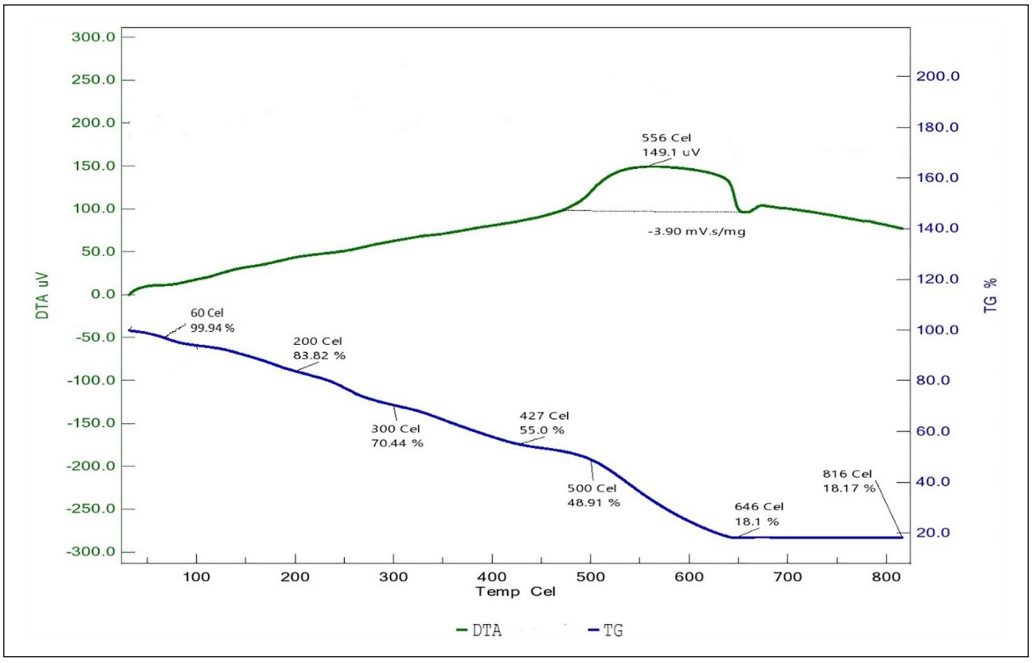

Figure 6. TGA and DTA curves of complex **1** $[VO(AcSHA)_2]$.

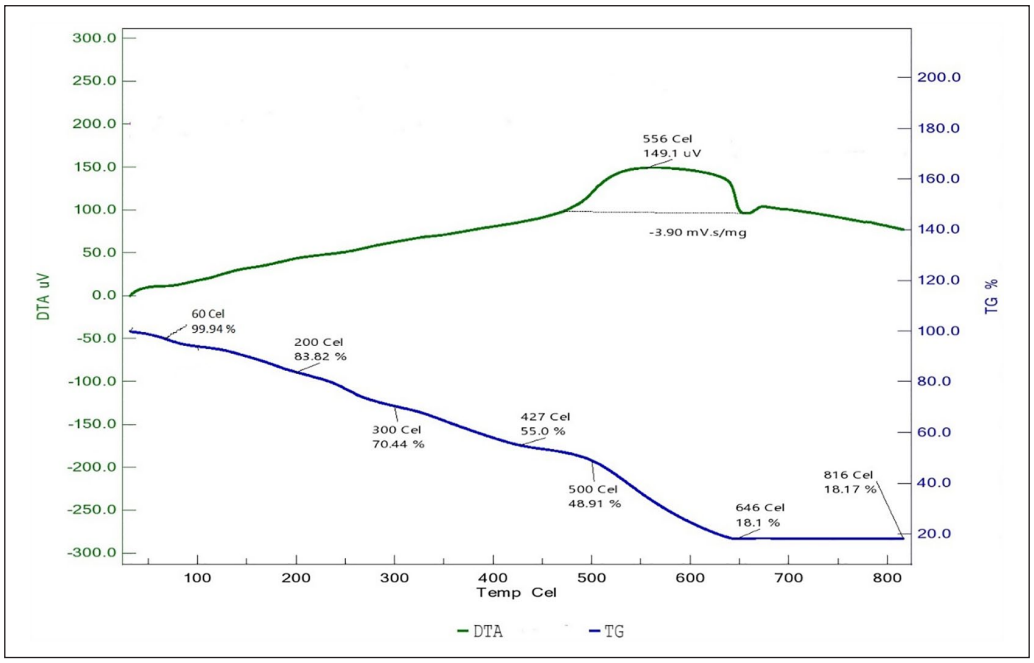

Figure 7. TGA and DTA curves of complex **2** [VO(acac)(ACSHA)].

Table 8. Thermal data of oxidovanadium(IV) complexes 1 and 2.

Complex	Initial decomposition temperature	Stages of decomposition	Observed mass loss (%)	Decomposition temperature range (°C)	Peak nature in DTA (exothermic, °C)	Decomposition product
$[VO(AcSHA)_2]$	60°C	I	45	60–427	–	[VO(AcSHA)]
		II	36.9	427–646	556	VO_2
[VO(acac)(AcSHA)]	85°C	I	57.73	85–400	133	[VO(acac)]
		II	27.57	400–617	577	VO_2

DTA: differential thermal analysis.

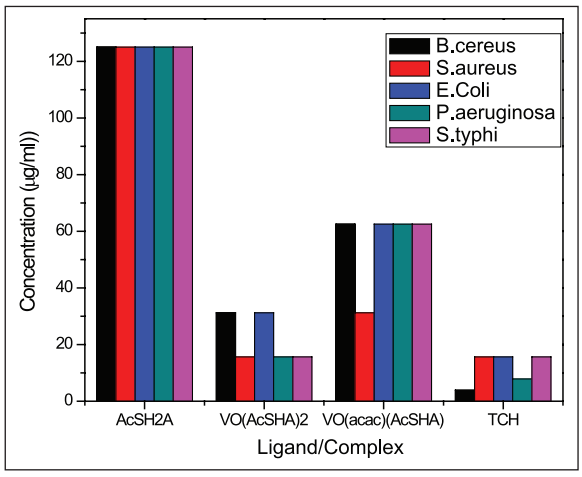

Figure 8. Bar diagram showing the in vitro antibacterial activity studies of the free ligand and the complexes **1** and **2.**

determined as V_2O_5 by decomposing the complex with a mixture of concentrated H_2SO_4 and concentrated HNO_3. The carbon, hydrogen, and nitrogen analyses were obtained using the CHN elemental analyzer (FLASH 2000; Thermo Scientific). The molar conductance (10^{-3} M solution in methanol) of the complexes was obtained using a conductivity bridge (Type CM-82T; Elico) at 25°C ± 0.1°C. At the room temperature, magnetic susceptibility was measured by Gouy's method,[76] using $Hg[Co(NCS)_4]$ as a calibrant. The IR spectra were recorded as KBr pellets using a FTIR spectrophotometer (PerkinElmer). Electronic spectra were recorded using a 100 Bio UV-Vis spectrophotometer (Varian Cary) in absolute ethanol. ESI mass spectra were recorded using a Micromass Quattro-TOF (Waters), with a mass range of 4000 amu in quadrupole and 20,000 amu in Tandem time-of-flight (TOF). At the room temperature, powder X-band ESR spectra were recorded using an E112 ESR spectrometer (Varian). The cyclic voltammetric measurements were performed at 25°C on an Autolab Potentiostat 128N electrochemical analyzer using a single compartmental cell of volume 10–15 mL, comprising a three-electrode system of a Pt-disk as the working electrode, Pt-wire as an auxiliary electrode, and Ag/AgCl electrode as the reference electrode. Potassium chloride (KCl; 0.4 M) was used as the supporting electrolyte in the methanol/H_2O (5:95) electrolyte system. Thermograms (TGA and DTA curves) of the complexes were recorded using a Diamond TG/DTA thermogravimetric analyzer (PerkinElmer) at a

Table 9. Antibacterial activity data determined by the MIC method.

Ligand/complex	MIC ± SD (μg/mL)				
	Gram-positive			Gram-negative	
	B. cereus	*S. aureus*	*E. coli*	*P. aeruginosa*	*S. typhi*
($AcSH_2A$)	125 ± 0.3	125 ± 0.5	125 ± 0.2	125 ± 0.04	125 ± 0.4
[$VO(AcSHA)_2$]	3.90 ± 0.2	15.63 ± 0.4	31.25 ± 0.05	15.63 ± 0.3	15.63 ± 0.05
[VO(acac)(AcSHA)]	62.5 ± 0.45	31.25 ± 0.02	62.5 ± 0.5	62.5 ± 0.2	62.5 ± 0.5
Tetracycline hydrochloride	7.84 ± 0.02	15.63 ± 0.01	15.63 ± 0.03	7.84 ± 0.4	15.63 ± 0.2

MIC: minimum inhibitory concentration; SD: standard deviation.

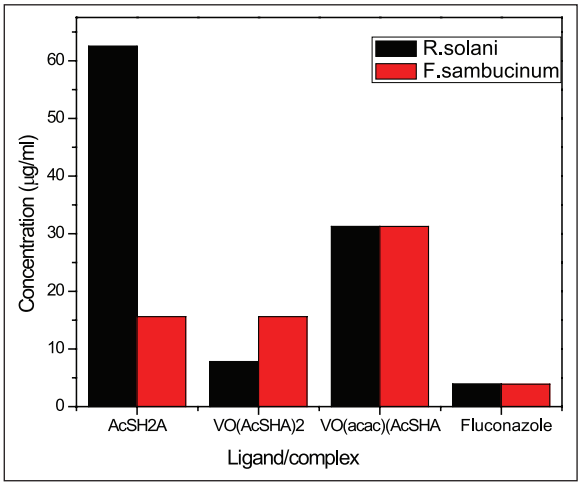

Figure 9. Bar diagram showing the in vitro antifungal activity studies of the free ligand and the complexes **1** and **2**.

Table 10. Antifungal activity determined by the MIC method.

Ligand/complex	MIC ± SD (μg/mL)	
	R. solani	*F. sambucinum*
($AcSH_2A$)	62.5 ± 0.3	15.62 ± 0.04
[$VO(AcSHA)_2$]	7.81 ± 0.01	15.62 ± 0.2
[VO(acac)(AcSHA)]	31.25 ± 0.5	31.25 ± 0.3
Fluconazole	3.90 ± 0.2	3.90 ± 0.01

MIC: minimum inhibitory concentration; SD: standard deviation.

Table 11. Antioxidant activity data of the free ligand and the complexes **1** and **2** using DPPH.

Ligand/complex	Scavenging potential (%)
($AcSH_2A$)	~4.9–26.3
[$VO(AcSHA)_2$]	~29.4–45.3
[VO(acac)(AcSHA)]	~10.4–43.28

heating rate of 10°C/min from ambient temperature to 800°C under an N_2 atmosphere.

Synthesis

Synthesis of ($AcSH_2A$). To pyridine (15 mL) was added salicylhydroxamic acid (5 g, 32.7 mmol), and the reaction mixture was stirred at room temperature to form an orange-colored solution. After cooling to 0°C, acetyl chloride (2.4 mL, 34 mmol) was added. The mixture was stirred at 0°C for 30 min, followed by stirring at room temperature.[75,77] To this solution, ethyl acetate (30 mL), 5% HCl (90 mL), and a saturated solution of sodium chloride (120 mL) were added. The aqueous phase was separated from the organic phase through separating funnel and dried over magnesium sulfate. The solvent was removed using a rotary evaporator to afford a cream-colored solid that was recrystallized from ethyl acetate.

Yield = 2.2 g (32%). Decomposition Temp. = 135°C. The formation of acetylsalicylhydroxamic acid [*N*-(acetoxy)-2-hydroxybenzamide] was established by the elemental analysis, IR, and ^{1}H nuclear magnetic resonance (NMR) spectroscopy. Anal. calcd for [$C_6H_4(OH)CONHOCOCH_3$]: C, 55.20; H, 4.90; N, 7.28; found: C, 54.85; H, 4.65; N, 7.00%. IR (KBr disk): 1805, 1795, 1650, 1620, 1200 cm^{-1}. ^{1}H NMR (MHz $CDCl_3$): δ 2.45 (s, 3H, CH_3) and 7–8 (m, 4H, ArH).

Synthesis of [$VO(AcSHA)_2$] from $VOSO_4.5H_2O$. To a solution of $VOSO_4.5H_2O$ (1 g, 3 mmol) in absolute ethanol (10 mL) was added 2 equiv. of $AcSH_2A$ (1.5 g, 7 mmol) dissolved in absolute ethanol (10 mL). The reaction mixture was stirred for 1 h and then refluxed for 8–10 h. The excess solvent was removed by distillation. To the concentrate was added petroleum ether (20 mL), and the product was dried under vacuum. A dark blue solid was obtained.

Yield = 1.2 g (67%), Decomposition Temp. = 145°C, Mol. Mass [$C_{18}H_{16}N_2O_9V$] = 457, Anal. calcd for [$C_{18}H_{16}N_2O_9V$]: C, 50.05; H, 4.35; N, 3.29; V; 14.32; found: C, 49.56; H, 4.00; N, 3.00; V, 13.98%. Λ_M (MeOH): 3.92 $Scm^2 mol^{-1}$; μ_{eff} (293 K): 1.70 BM.

Synthesis of [VO(acac)(AcSHA)] from [$VO(acac)_2$]. To a solution of $VO(acac)_2$ (0.5 g, 1 mmol) in absolute ethanol (10 mL) was added 2 equiv. of $AcSH_2A$ (1 g, 5 mmol) dissolved in absolute ethanol (10 mL). The reaction mixture was stirred for 1 h and then refluxed for 8–10 h. The excess solvent was removed by distillation. To the concentrate was added petroleum ether (20 mL), and the product was dried under vacuum whereupon a dark blue complex was formed.

Yield = 0.50 g (72%), Decomposition Temp. = 157°C, Mol. Mass [$C_{14}H_{15}NO_7V$] = 360, Anal. calcd for [$C_{14}H_{15}NO_7V$]: C, 50.40; H, 4.27; N, 3.25; V; 14.50; found: C, 50.06; H, 3.95; N, 3.05; V, 13.90%. Λ_M (MeOH): 3.90 $Scm^2 mol^{-1}$; μ_{eff} (293 K): 1.72 BM.

Biological assay

Antibacterial activity. The free ligand $AcSH_2A$ and the oxidovanadium(IV) complexes $[VO(AcSHA)_2]$ and [VO(acac)(AcSHA)] were screened in vitro for the antibacterial and antifungal activity against the selected Gram-positive bacteria (*S. aureus* and *B. cereus*), Gram-negative bacteria (*E. coli, P. aeruginosa*, and *S. typhi*), and fungi (*R. solani* and *F. sambucinum*) at different concentrations in dimethyl sulfoxide (DMSO) employing the MIC method.[78,79] The MIC is the lowest concentration of the antimicrobial agent that prevents the development of visible growth of microbes after overnight incubation. The samples were tested in triplicate.

Method. A sterile flat bottom 96-well microtiter plate was labeled as 1–7, in which wells 1–5 are allotted for the test sample, 6 for the positive control (broth + standard antibiotic (2 µL) + microorganism), and 7 for the negative control (broth + microorganism). Then, 30 µL of media was added to each well, including the positive and negative controls. A stock solution of the sodium salt of Resazurin dye as an indicator (0.02% (wt/mol); Sigma Aldrich)[80] was prepared in distilled water, filtered, sterilized, and stored at 4°C for 1 week. This dye (5 µL) was added to each well. The test samples were added in twofold dilution to wells (1–5). The plates were then wrapped with aluminum foil and incubated at 37°C for 24 h in the case of bacteria and at 28°C for 72 h for fungi. A change in color in the wells of the positive control indicated the proper growth of the isolate, and no change in color of wells of the negative control indicated the absence of contaminants. The results were compared with the standard antibacterial drug tetracycline hydrochloride and the antifungal drug fluconazole.

Statistical analysis. Statistical analysis was performed using the standard t-test, and $p < 0.05$ was considered significant. The data are represented as standard deviation.

Antioxidant activity. The free radical scavenging activity of the complexes is measured in terms of hydrogen donation or radical scavenging ability using the stable DPPH radical as described by Blois.[81] DPPH is usually used as a substrate to evaluate antioxidant activity. DPPH (1,1-diphenyl-2-picrylhydrazyl) having an unpaired electron displays a strong absorption band at 517 nm, which decreases stoichiometrically upon pairing of the electron.[82,83] A change in the absorbance produced in the reaction is widely used to test the ability of molecules to act as free radical scavengers. The newly synthesized oxidovanadium complexes in +4 oxidation state can donate an electron to reduce the DPPH radical to DPPH (α,α-diphenyl-β-picrylhydrazine), and the VO(IV) ion is oxidized to VO(V). The stock solutions of the complexes (0.001 g/mL) were prepared in DMSO, from which different concentrations (20–100 µL) being prepared. A solution of DPPH (0.1 mmol) in methanol was prepared, and 1 mL of this solution was added to each of the test solutions. The mixture was shaken vigorously and incubated for 30 min. The absorbance was measured at 517 nm. All the tests were carried out in triplicate. Ascorbic acid was used as a standard or positive control. The ability to scavenge the DPPH radical was calculated using the following equation

$$I(\%) = \left(\frac{A_{control} - A_{sample}}{A_{control}} \right) \times 100$$

where $A_{control}$ is the absorbance of the control, and A_{sample} is the absorbance of the sample.

Acknowledgements

The authors thank the IIT Mandi for recording Fourier-transform infrared spectroscopy (FTIR), mass spectra, and elemental analyses. The authors gratefully acknowledge the support of the Department of Biotechnology, Himachal Pradesh University, Shimla, for providing laboratory facilities to carry out biological studies.

Declaration of conflicting interests

The author(s) declared no potential conflicts of interest with respect to the research, authorship, and/or publication of this article.

Funding

The author(s) received no financial support for the research, authorship, and/or publication of this article.

ORCID iD

Neeraj Sharma https://orcid.org/0000-0002-5410-6674

Supplemental material

Supplemental material for this article is available online.

References

1. Wai-Yin Sun R, Ma D-L, Wong EL-M, et al. *Dalt Trans* 2007; 4884.
2. Rehder D. *Inorganica Chim Acta* 2017; 455: 378–389.
3. Pessoa JC, Etcheverry S and Gambino D. *Coord Chem Rev* 2015; 301–302: 24–48.
4. Rehder D. *Dalt Trans* 2013; 42: 11749.
5. Crans DC. *J Org Chem* 2015; 80: 11899–11915.
6. Kiss T, Enyedy ÉA and Jakusch T. *Coord Chem Rev* 2017; 352: 401–423.
7. Sanna D, Buglyó P, Micera G, et al. *JBIC J Biol Inorg Chem* 2010; 15: 825–839.
8. Adam AMA, Naglah AM, Al-Omar MA, et al. *Int J Immunopathol Pharmacol* 2017; 30: 272–281.
9. Devi RKB, Devi SP and Singh RKH. *Spectrosc Lett* 2012; 45: 93–103.
10. Sasmal PK, Saha S, Majumdar R, et al. *Inorg Chem* 2010; 49: 849–859.
11. Butenko N, Tomaz AI, Nouri O, et al. *J Inorg Biochem* 2009; 103: 622–632.
12. Evangelou AM. *Crit Rev Oncol Hematol* 2002; 42: 249–265.
13. Martínez Medina JJ, Naso LG, Pérez AL, et al. *J Inorg Biochem* 2017; 166: 150–161.
14. Naso LG, Lezama L, Valcarcel M, et al. *J Inorg Biochem* 2016; 157: 80–93.
15. Savithri K and Revanasiddappa HD. *Bioinorg Chem Appl* 2018; 2018: 1–12.

16. Fernández M, Becco L, Correia I, et al. *J Inorg Biochem* 2013; 127: 150–160.
17. Fernández M, Varela J, Correia I, et al. *Dalt Trans* 2013; 42: 11900.
18. Scalese G, Benítez J, Rostán S, et al. *J Inorg Biochem* 2015; 147: 116–125.
19. Machado P, de A, Mota VZ, et al. *Acta Trop* 2015; 148: 120–127.
20. Maurya MR, Haldar C, Khan AA, et al. *Eur J Inorg Chem* 2012; 2012: 2560–2577.
21. Correia I, Adão P, Roy S, et al. *J Inorg Biochem* 2014; 141: 83–93.
22. D'Cruz OJ and Uckun FM. *J Appl Toxicol*; 21: 317–22.
23. Chien P-S, Mak O-T and Huang H-J. *Biochem Biophys Res Commun* 2006; 339: 562–568.
24. Chakraborty T, Swamy AHMV, Chatterjee A, et al. *J Cell Biochem* 2007; 101: 244–258.
25. Baran EJ. *J Braz Chem Soc* 2003; 14: 878–888.
26. Winter PW, Al-Qatati A, Wolf-Ringwall AL, et al. *Dalt Trans* 2012; 41: 6419.
27. Peters KG, Davis MG, Howard BW, et al. *J Inorg Biochem* 2003; 96: 321–330.
28. Thompson KH, Lichter J, LeBel C, et al. *J Inorg Biochem* 2009; 103: 554–558.
29. Martins PGA, Mori M, Chiaradia-Delatorre LD, et al. *ACS Med Chem Lett* 2015; 6: 1035–1040.
30. Treviño S, Díaz A, Sánchez-Lara E, et al. *Biol Trace Elem Res* 2019; 188: 68–98.
31. Sharma D, Revanasiddappa HD, Kumar BCV, et al. *Biointerface Res Appl Chem* 2019; 9: 3776–3782.
32. La M, Wang P-P and Xue L-W. *Inorg Nano-Metal Chem* 2019; 1–5.
33. Lima S, Banerjee A, Mohanty M, et al. *New J Chem* 2019; 43: 17711–17725.
34. Edwards DC and Myneni SCB. *J Phys Chem A* 2005; 109: 10249–10256.
35. Agarwal YK and Sharma CK. *Indian J Chem* 2007; 46A: 1772–1777.
36. Bauer L and Exner O. *Angew Chemie Int Ed English* 1974; 13: 376–384.
37. Muri EMF, Nieto MJ, Sindelar RD, et al. *Curr Med Chem* 2002; 9: 1631–1653.
38. Senger J, Melesina J, Marek M, et al. *J Med Chem* 2016; 59: 1545–1555.
39. Ugwu DI, Ezema BE, Eze FU, et al. *Am J Org Chem* 2014; 4: 26–51.
40. Veysel T and Yılmaz FY. *Transit Met Chem* 1999; 24: 726–729.
41. Loll PJ, Sharkey CT, O'Connor SJ, et al. *Mol Pharmacol* 2001; 60: 1407–1413.
42. Dessì A. *J Inorg Biochem* 1992; 48: 279–287.
43. Sharma S and Sharma N. *Der Chem Sin* 2013; 4: 108–119.
44. Sharma S and Sharma N. *Der Chem Sin* 2013; 4: 87–96.
45. Sharma N, Kumar V, Sharma R, et al. *Bull Chem Soc Jpn* 2011; 84: 855–861.
46. Kumar A, Priya B, Thakur A, et al. *Adv Sci Eng Med* 2018; 10: 27–37.
47. Priya B, Sharma M, Sood S, et al. *Adv Sci Eng Med* 2018; 10: 129–136.
48. Geary WJ. *Coord Chem Rev* 1971; 7: 81–122.
49. Figgis BN. *Introduction to ligand fields*. London; New York: John Wiley & Sons Ltd, 1966.
50. Ballhausen CJ and Gray HB. *Inorg Chem* 1962; 1: 111–122.
51. Stoklosa HJ, Wasson JR and McCormick J. *Inorg Chem* 1974; 13: 592–597.
52. Cheng SH, Sheen SR, Cheng CP, et al. *Inorganica Chim Acta* 1990; 171: 21–24.
53. Raman N, Raja SJ, Joseph J, et al. *Russ J Coord Chem* 2007; 33: 7–11.
54. Sheela A, Sarada NC and Vijayaraghavan R. *Med Chem Res* 2013; 22: 2929–2937.
55. Kianfar AH and Mohebbi S. *J Iran Chem Soc* 2007; 4: 215–220.
56. Botto I, Vassallo M, Baran E, et al. *Mater Chem Phys* 1997; 50: 267–270.
57. Levina A, Crans DC and Lay PA. *Coord Chem Rev* 2017; 352: 473–498.
58. Levina A and Lay PA. *Chem—Asian J* 2017; 12: 1692–1699.
59. Gonçalves G, Tomaz I, Correia I, et al. *Dalt Trans* 2013; 42: 11841.
60. Costa Pessoa J, Gonçalves G, Roy S, et al. *Inorganica Chim Acta* 2014; 420: 60–68.
61. Costa Pessoa J. *J Inorg Biochem* 2015; 147: 4–24.
62. Le M, Rathje O, Levina A, et al. *JBIC J Biol Inorg Chem* 2017; 22: 663–672.
63. Doucette KA, Hassell KN and Crans DC. *J Inorg Biochem* 2016; 165: 56–70.
64. Jakusch T, Costa Pessoa J and Kiss T. *Coord Chem Rev* 2011; 255: 2218–2226.
65. Jakusch T and Kiss T. *Coord Chem Rev* 2017; 351: 118–126.
66. Sanna D, Micera G and Garribba E. *Inorg Chem* 2009; 48: 5747–5757.
67. Sanna D, Ugone V, Micera G, et al. *Dalt Trans* 2017; 46: 8950–8967.
68. Sanna D, Palomba J, Lubinu G, et al. *J Med Chem* 2019; 62: 654–664.
69. Mehtab S, Gonçalves G, Roy S, et al. *J Inorg Biochem* 2013; 121: 187–195.
70. Gaballa AS, Teleb SM, Asker MS, et al. *J Coord Chem* 2011; 64: 4225–4243.
71. Hassan LR, Ramasamy K, Lim SM, et al. *J Teknol* 2018; 80: 6.
72. Chohan ZH, Supuran CT and Scozzafava A. *J Enzyme Inhib Med Chem* 2004; 19: 79–84.
73. Chohan ZH, Mahmood-ul-Hassan Khan KM and Supuran CT. *J Enzyme Inhib Med Chem* 2005; 20: 183–188.
74. Rowe RA and Jones MM. In: *Inorganic Syhtheses*, 1957, p. 114.
75. O'Brien EC, Le Roy S, Levaillain J, et al. *Inorganica Chim Acta* 1997; 266: 117–120.
76. Hilal OM and Fredericks GE. *J Chem Soc* 1954; 785.
77. Traynham JG and Pascual OS. *J Org Chem* 1956; 21: 1362–1365.
78. Greenwood D, Slack R, Peutherer JF, et al. Medical microbiology: A guide to microbial infections: Pathogenesis, immunity, laboratory diagnosis and control. *Churchill Livingstone*, 2007.
79. Mackie TJ, Collee JC and McCartney JE. *Practical medical microbiology*. Edinburgh: Churchill Livingstone, 1989.
80. Khalifa RA, Nasser MS, Gomaa AA, et al. *Egypt J Chest Dis Tuberc* 2013; 62: 241–247.
81. Blois MS. *Nature* 1958; 181: 1199–1200.
82. Ilhan-Ceylan B, Tuzun E, Kurt Y, et al. *J Sulfur Chem* 2015; 36: 434–449.
83. Ibrahim MM, Mersal GAM, Ramadan A-MM, Shaban SY, et al. *J Mol Struct* 2017; 1137: 742–755.